JOURNAL OF MATERIALS SCIENCE 26 (1991) 4095–4103

Fracture characteristics of cement-stabilized soils

J. DAVIES
Department of Civil Engineering and Building, The Polytechnic of Wales, Llantwit Road, Pontypridd, CF37 1DL, UK

Fracture characteristics of cement-stabilized soil under Mode I (tensile) and Mode II (in-plane shear) were investigated on a series of cube specimens. The linear elastic fracture mechanics approach was applied to study the stress distribution in the specimens and also to determine the constitutive equations for fracture parameters K_I and K_{II}. The experimental studies were carried out on a range of 100 mm soil–cement cube specimens modified for fracture testing by inserting a series of slots. It was shown that results predicted by numerical models were in acceptable agreement with the experimental observations. The fracture parameter K_I was found to be in the range 0.11–0.17 MN m$^{-3/2}$ and the parameter K_{II} in the range 0.31–0.45 MN m$^{-3/2}$. This result indicated that the soil–cement exhibited a greater resistance to shear fracture than was expected.

Nomenclature

K	Stress intensity factor:
σ	elastic stress field near the crack tip.
$f(a/w)$	Dimensionless parameter depending on geometries of the specimen and the crack.
r	Radial distance measured from the crack tip.
U	Area under load–deflection graph.
dU	Difference in potential energy for unit thickness between two identically loaded bodies.
dA	Increase in crack area.
G	Strain energy release rate.
E	Young's modulus.
ν	Poisson's ratio.
a	Crack length.
w	Specimen width.
B	Specimen thickness.
H	Slot separation.
σ_y	Yield stress of material.
K_I, K_{II}	Fracture toughness in Mode I, Mode II.
P	Applied load.
P_{max}	Load at failure.
τ	In-plane shear stress.

1. Introduction

1.1. Soil–cement

This hardened material is formed by curing and compacting a mixture of pulverized soil, a small percentage of cement and water. Sufficient cement is added to the soil to harden it, and the moisture content of the mixture must be adequate for compaction and hydrating the cement. The most important use of soil–cement is as a roadbase and/or a subbase material in roadways, airport runways, taxiways and aprons. It has also been used as a foundation material for large structures and in the construction of low-cost buildings in arid climates.

As in concrete, the strength of soil–cement increases with time. The development of strength begins as soon as water and cement are mixed; construction with soil–cement must be done according to a carefully controlled schedule. In general, the more efficiently cement, water and soil are mixed, the greater will be the stability and durability of the soil–cement product. The conditions under which curing takes place have a considerable effect on the degree of stabilization of soil by cement. Soil–cement must be moist-cured during the initial stages of its life so that sufficient moisture can be maintained in the mixture to meet hydration needs. The temperature during curing has a considerable effect, and higher strengths are obtained at higher curing temperatures.

Cracking and ultimately the failure of roads, pavement systems and similar structures is often associated with cracking or failure of the subbase. It is important that the fracture properties and behaviour of soil–cement under varying types of loading are fully understood, and consequently this knowledge could be used to improve design and selection of subbase materials. A better understanding of interaction of the above factors and materials behaviour and responses to varying loading regimes, may provide answers to structural problems which may be induced by cracking.

1.2. The concept of fracture mechanics

From an engineering point of view the main objective in developing fracture mechanics concepts is to relate the development of fracture, its orientation and ultimate failure to the applied state of stresses. The resistance of material to the propagation of existing crack is

0022–2461/91 $03.00 + .12

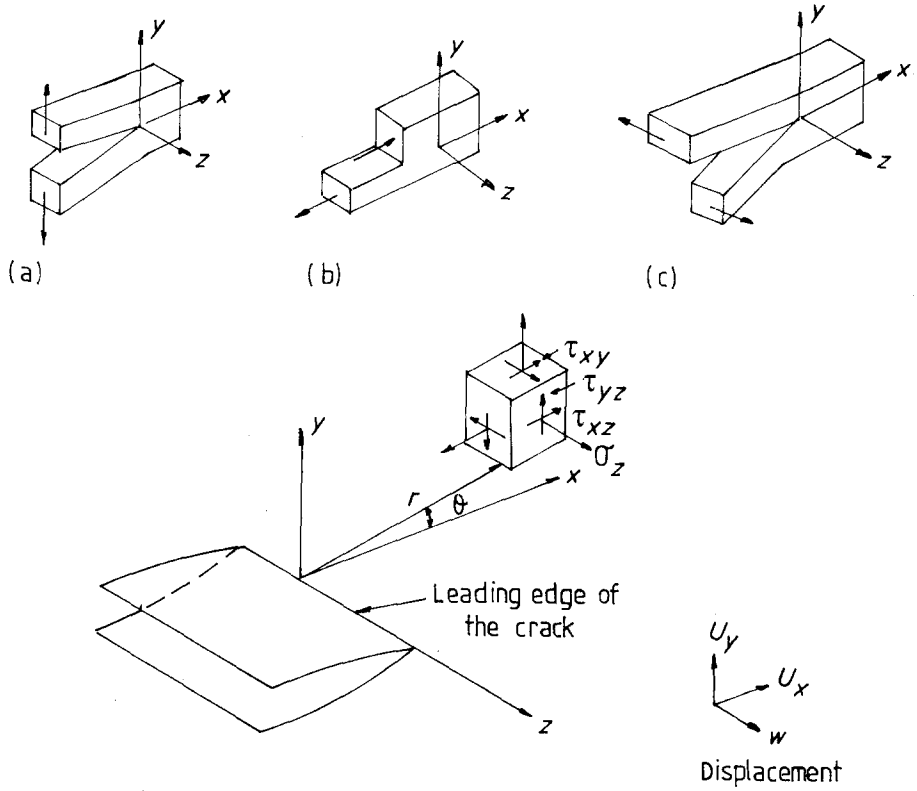

Figure 1 Modes of failure and notation of the crack tip region. (a) Mode I, opening mode; (b) Mode II, sliding mode; (c) Mode III, tearing mode.

known as fracture toughness, the magnitude of which can be assessed by varying approaches.

There are three basic modes of failure, see Fig. 1. Mode I (tensile), Mode II (in-plane shear) and Mode III (antiplane shear). The elastic stress field near the crack tip is proportional to the stress intensity parameter, K, ($K = f(a/w)\sigma(\pi r)^{-1/2}$) depending on the type of loading and the geometry of the cracked body.

The stress intensity factor, K, is thus a measure of the mechanical properties in the presence of a crack in the same way as stress characterizes the mechanical properties of an uncracked specimen. Small-scale non-linear effects, such as those due to yielding, micro-structural and local irregularities in the crack surface do not affect the general character of the elastic stress field and can be neglected in a reasonable approximation. Stress intensity factors can be computed for varying crack configurations and therefore provide a useful means for the study of fracture processes.

The rate of energy absorption, G, at any stage in the crack growth can be determined as dU/dA, where dA is the increase in crack area. The crack will grow when the stress in the specimen has been raised sufficiently for these parameters to reach their critical values, K_c and G_c (the critical stress intensity factor and the critical strain energy release rate) and either can be used as a measure of the resistance of the material to cracking known as materials toughness. Irwin [1] established that for linear elastic materials, K and G are related through the relationship

$$K^2 = EG \quad \text{for plane stress} \quad (1a)$$

$$K^2 = EG/(1 - \nu^2) \quad \text{for plane strain} \quad (1b)$$

where E is Young's modulus and ν is Poisson's ratio.

Application of linear elastic fracture mechanics (LEFM) to concrete was first attempted by Kaplan [2] and since then a large number of investigators have examined the applicability of LEFM to concrete or cementitious materials [3–13]. The results of these investigations show that when fracture toughness is evaluated from notched specimens using LEFM a significant size effect is observed [14–16]. This is attributed to non-linear slow crack growth that occurs prior to the peak load. The material used in this investigation, however, is fine-grained soil, stabilized with cement and, due to a near linear stress–strain relationship, this material was assumed to be linear elastic.

It is generally accepted that the fracture in cementitious materials is initiated when tensile stresses over a fracture process zone reach a critical value, rather than the value at some point, as it is in the case of homogeneous and elastic materials.

The object of this study was to obtain and improve understanding of fracture processes in soil–cement subjected to varying loading conditions and clarify the basis that can be used to describe the crack initiation and propagation in this material media.

1.3. Models used in the numerical study of fracture characteristics of cement-stabilized soil

Linear elastic finite element analysis was used to study the fracture behaviour of soil–cement specimens. The plane strain analyses were carried out using eight- and six-noded isoparametric elements together with the distorted "crack tip" element (with the mid-side node

adjacent to the crack tip which moved to the 1/4 position) to represent the elastic stress singularity at the crack tip. The numerical modelling and analysis were carried out on VAX 11/785 computer with the aid of PAFEC–FE interactive system. Two basic geometries were considered.

1. Split-cube specimen: this geometry was used extensively by Barr and Sabir [17, 18] in the study of fracture characteristics of Mode I (tensile) in concrete, Fig. 2.

2. Punch-through shear specimen: investigated by the present author and co-workers [19–21] and used in the study of fracture characteristics of mixed-mode in concrete and mortar, Fig. 3.

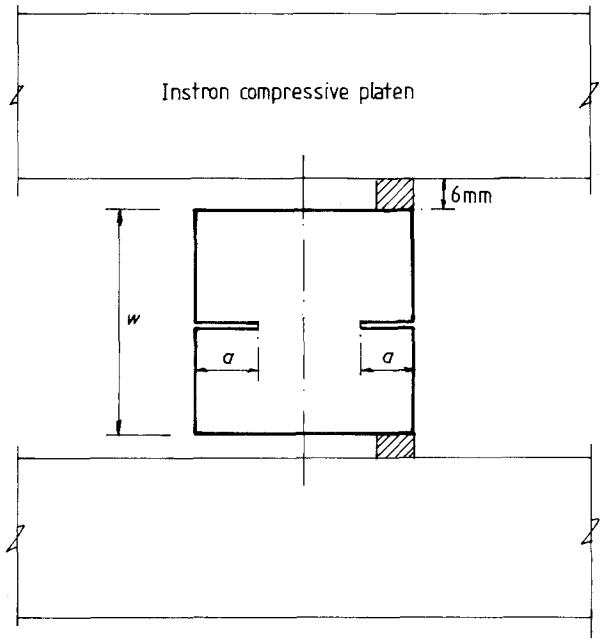

Figure 2 Specimen geometry for Mode I testing: split-cube specimen.

The knowledge and understanding of the cracking process and the magnitude of fracture parameters of soil–cement are important factors if better quality and improved resistance to cracking is required. Detailed analyses of both specimens are discussed elsewhere [21–23]; therefore only some results will be given in this report.

1.3.1. Split-cube specimen

The whole specimen with $a = 30$ mm shown in Fig. 2 was subdivided into 1280 six- and eight-noded isoparametric elements, with the smallest elements in the crack-tip region being of the order of $0.005a$. Fig. 4 shows the contours of maximum principal stresses in the specimen. It can be seen that a high tensile stress concentration occurs at the notch remote from the load, the condition required to initiate tensile fracture. It is generally accepted that the tensile fracture propagates in the direction perpendicular to the maximum principal tensile stresses. Fig. 5 shows the predicted direction of the maximum principal tensile stresses superimposed with the crack path as observed and recorded from the experiments. It can be seen that the observed crack path follows fairly closely the direction perpendicular to the direction of the maximum tensile stress, therefore indicating that the tensile failure mode, Mode I, most likely occurred in this specimen.

The constitutive equation describing the variation of Mode I stress intensity factor, K_I, with the specimen geometry was determined by Sabir [18] as

$$K_I = \frac{P}{Bw^{1/2}}[18.3(a/w)^{1/2} - 430.0(a/w)^{3/2} + 3445.2(a/w)^{5/2} - 11\,075.8(a/w)^{7/2} + 12\,966.8(a/w)^{9/2}] \quad (2)$$

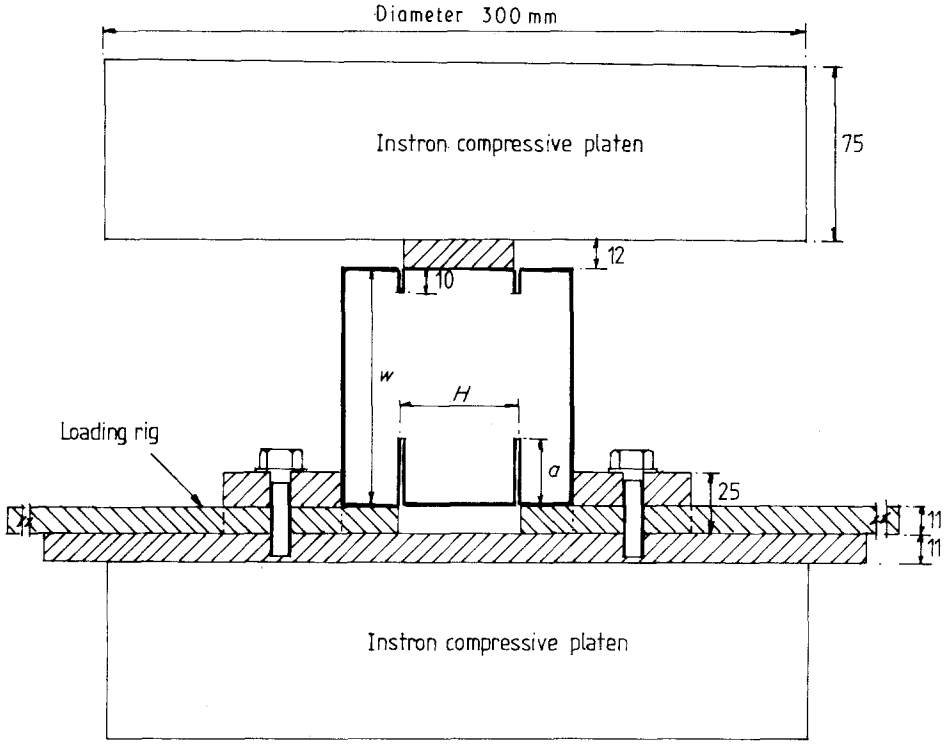

Figure 3 Specimen geometry for Mode II testing: punch-through shear specimen.

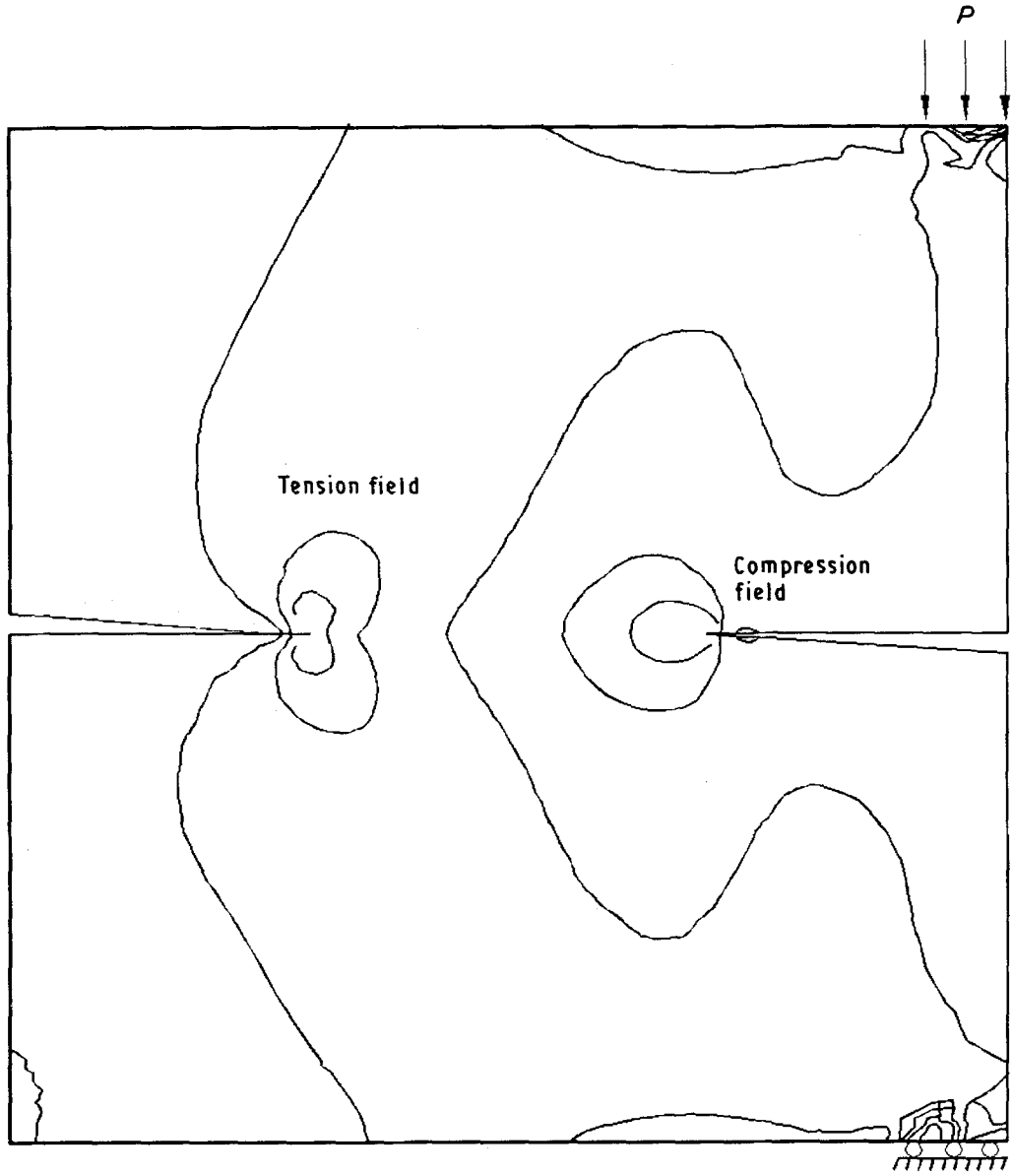

Figure 4 Maximum principal stress contours: split-cube specimen.

and was used in the evaluation of the fracture parameter K_I for soil–cement cubes during this investigation.

1.3.2. Punch-through shear specimen

The geometry of this specimen and the type of loading are designed to generate very high shear stress concentrations in the ligament with notches and therefore to force material to fail in punching shear. 974 six- and eight-noded isoparametric elements were used in the analysis of one-half of the specimen with the special crack tip element at the crack tips. Fig. 6 represents the variation of σ_x, σ_y and τ_{xy} stresses between the top and bottom notches. The high shear stress concentration may be seen in the region of both notches and the fairly uniform shear stress field in the centre of the ligament was achieved.

Fig. 7 shows the directions of the maximum tensile principal stress vectors occurring in the punch-through shear specimen. As can be seen, the directions of these stresses are of distinctly inclined nature and it would therefore be expected that the fracture path would follow this inclined direction. Experimental observations indicated, however, that the fracture path was almost vertical, see Fig. 7. Similar observations were made when fracture studies of mortar were carried out and it was suggested that the mixed-mode type of failure with a predominant shear component was taking place in this specimen geometry; more detailed information can be found in [23, 24]. Numerical analysis [24], utilizing fracture mechanics principles, showed that the stress intensity factor, K_{II} (shear component), was about 60 times higher than K_I (tensile component). The stress intensity factor, K_{II}, determined from the numerical analysis is given by

$$K_{II} = 0.89 \frac{P}{Bw} (\pi a)^{1/2} \quad (3)$$

Numerical analyses of both specimen geometries together with experimental observations indicated that two distinctly different failure mechanisms were taking place in these specimens, one producing Mode I and another mixed-mode with a shear component so significant that the failure mechanism was assumed to be Mode II.

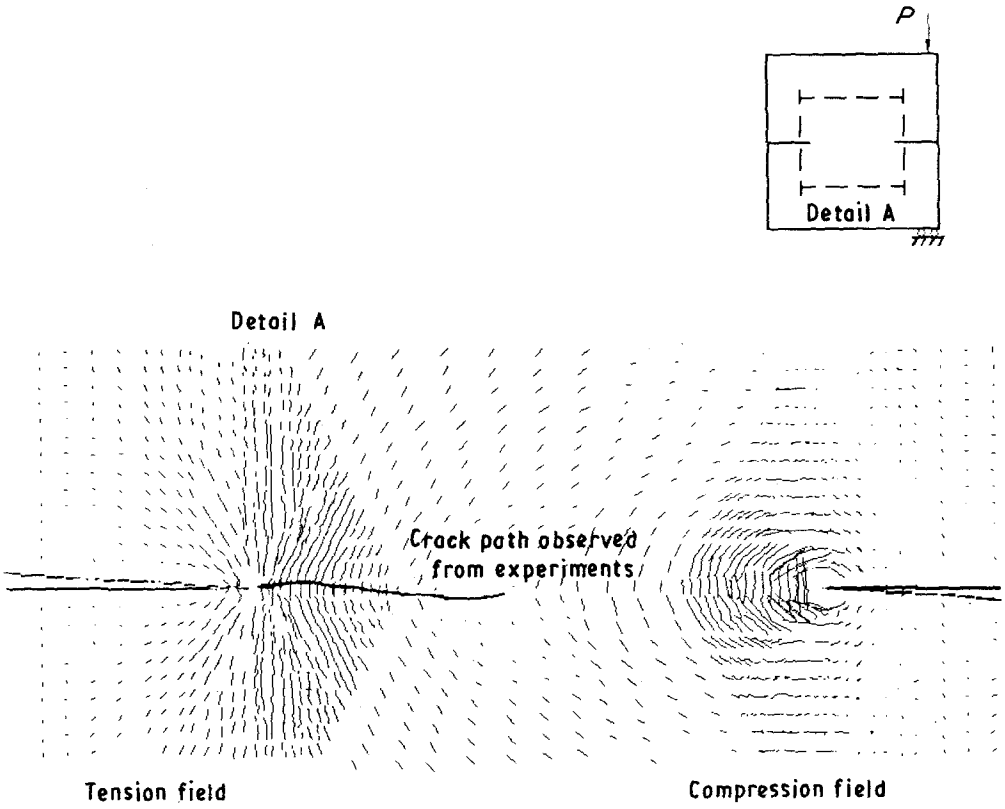

Figure 5 Maximum principal stress vectors directions and observed crack path: split-cube specimen.

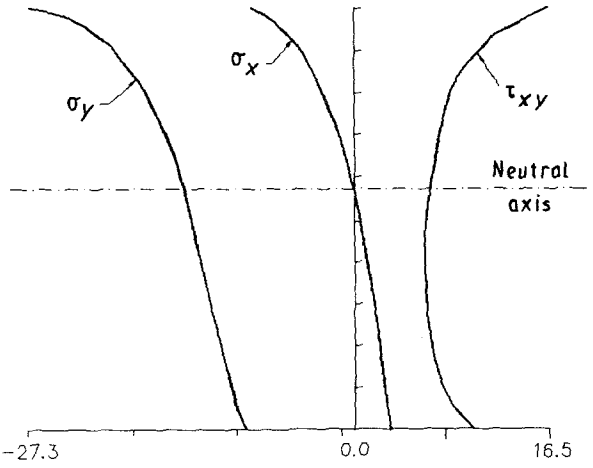

Figure 6 Variation of directional stresses: punch-through shear specimen.

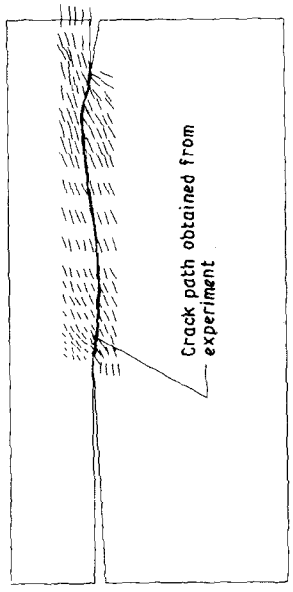

Figure 7 Maximum principal stress vectors directions and observed crack path: punch-through shear specimen.

2. Material and sample preparation

2.1. Preparation of soil–cement

The soil used in this investigation was a red marl (Keuper) from Leckwith, Cardiff, South Wales. The marl had been dried in the oven and pulverized into a powder form and 8% by weight of ordinary Portland cement was added. Because moisture content is an important factor in soil properties, it was necessary to determine this.

The standard Proctor compaction test was used to determine the optimum dry density and moisture content of the soil–cement according to BS 1924 [25]. The details of the test are summarized in Tables I and II, the optimum moisture content was found to be 16.6% at a dry density of 1.78 Mg m^{-3} as tabulated in Table III. In order to maintain consistency the follow-

TABLE I Weight of water required for the Proctor compaction test

Percentage of water (%)	Weight of water (g)	Increment of water (g)
14	453.6	453.6
17	550.8	97.2
20	648.0	97.2
23	745.2	97.2
26	842.4	97.2
29	939.6	97.2

TABLE II Values obtained from the Proctor compaction test

	Container number					
	8	17	19	23	72	88
% of water	14	17	20	23	26	29
Mass of container, m_1	9.44	9.42	16.14	10.15	9.98	10.10
Mass of wet soil + container, m_2 (g)	48.24	47.77	49.30	54.19	48.26	67.14
Mass of dry soil + container, m_3 (g)	43.54	42.41	43.98	46.22	40.61	54.72
Mass of moisture, $m_2 - m_3$ (g)	4.70	5.36	5.32	7.97	7.65	12.42
Mass of dry soil, $m_3 - m_1$ (g)	34.10	32.99	27.84	36.07	30.63	44.62
Moisture content, $W = \left(\frac{m_2 - m_3}{m_3 - m_1}\right) \times 100\%$	13.78	16.25	19.11	22.10	24.98	27.84
Mass of mould + base, M_1 (g)	3017	3017	3017	3017	3017	3017
Mass of mould + base + compacted soil, M_2 (g)	4979	5096	5104	5043	4993	4904
Mass of compacted soil, $M_2 + M_1$ (g)	1962	2079	2087	2026	1976	1887
Bulk density, $\rho = \frac{(M_2 - M_1)}{1000}$ ($Mg\,m^{-3}$)	1.962	2.079	2.087	2.026	1.976	1.887
Dry density $= \frac{100\rho}{100 + W}$ ($Mg\,m^{-3}$)	1.72	1.79	1.75	1.66	1.58	1.48

TABLE III General properties of soil–cement (8%)

Liquid limit	22.4% MC
Plastic limit	15.2% MC
Moisture content	16.6%
Optimum dry density	1.78 $Mg\,m^{-3}$
Elastic modulus, E	1200.0 $N\,mm^{-2}$
Poisson's ratio, ν	0.25
Compressive strength	4.96 $MN\,m^{-2}$

ing mix was adopted: red marl 4 kg, cement (8%) 0.32 kg, water (18%) 0.778 kg.

The soil–cement was compacted in standard 100 mm concrete cube moulds with a "collar", made by removing the base from another mould attached to the top by means of two "G" clamps. The soil–cement was broken up into granular form before being placed into the bottom of the mould. This first procedure proved to be of vital importance because lumps of the material at the bottom of the mould did not compact well. The cubes were filled and hand compacted gently with a 5 mm diameter steel rod in five equal layers. A 100 mm square × 300 mm long piece of timber was then placed on to the top of the material. To produce constant compaction, a "Kango" hammer which gives 2000 blows/min was used. It was found that 15 s operating time produced a desired uniform consistency and this compaction method was used throughout the investigation. After compaction, the collar was removed and the extra material was levelled off with a spatula.

The curing temperature was kept constant at 22 °C and precautions were taken to control the moisture content. The soil–cement cubes in their moulds were enclosed in sealed polythene bags for 24 h. The moulds were then stripped and the cubes were firstly wrapped in cling film, then in tin foil and sealed in polythene bags for 28 days.

The compressive strength of 100 mm soil–cement cubes was determined according to BS 1881: Part 116 using the Avery Denison 7226 testing machine. The average compressive strength was found to be 4.96 $MN\,m^{-2}$. The elastic modulus and Poisson's ratio were determined using a standard testing procedure according to BS 1881: Part 116 [26] and was found to be 1.2 $kN\,mm^{-2}$ and 0.25 respectively, see Table III.

2.2. Insertion of notches and testing machine details

The quality of inserted notches will affect considerably the fracture tests results and it is therefore important that the notch insertion technology is capable of producing accurate and reproducible slots. Both the split-cube and punch-through shear specimens were notched after 21 days using a circular lathe mounted with a diamond-edge cutting blade. This technology enabled the insertion of slots less than 2 mm wide to be controlled to a high degree of accuracy. The notches were inserted in a perpendicular direction to the layers of compaction.

All of the fracture tests were carried out at nominal room temperature in the Instron 1251 testing machine having a stiffness 750 $kN\,mm^{-1}$ ± 10%, using displacement control in the dynamic testing mode. The specimens were positioned between the platens as shown in Figs 2 and 3. The top platen was stationary while the bottom platen moved at a constant rate of 0.003 $mm\,s^{-1}$ upwards; the load–displacement curves were recorded autographically on a chart.

3. Results

3.1. Mode I testing and fracture parameters

The 100 mm × 100 mm double-notched (split cube) test specimens were prepared as described in the previous sections, the notch depths being a = 20, 25, 30 and 35 mm. Eighteen specimens of each geometry were tested under the controlled conditions. It is important to note that for a valid fracture toughness

TABLE IV Mean fracture toughness values K_{Ic} for 100 mm eccentrically loaded double-notched cube soil–cement after 28 days

Test no.	a (mm)	Failure load (kN)	Equation 2, K_{Ic} (MN m$^{-3/2}$)
1	25	1.80	0.17
2		1.25	0.12
3		1.68	0.16
4		1.22	0.11
5	30	1.57	0.15
6		1.41	0.13
7		1.27	0.12
8		1.70	0.16
9		1.13	0.11
10	35	1.7	0.16
11		1.85	0.17
12		1.19	0.11

testing, the minimum specimen thickness must satisfy the condition $B \geqslant 2.5(K_{Ic}/\sigma_y)^2$ where K_{Ic} is the fracture toughness and σ_y is a yield strength of the material. In the case of soil–cement, assuming $K_{Ic} = 0.17$ MN m$^{-3/2}$ and $\sigma_y = 5$ MN m^{-2}, the required thickness $B \geqslant 3$ mm which confirms that the 100 mm cube specimen would represent the plane strain conditions required in the fracture toughness testing procedure.

The specimens were subjected to eccentric loading as shown in Fig. 2, the load being applied via two 6 mm square steel bars positioned along the edge of the specimen. This loading arrangement would generate a high tensile field at the notch tip remote from the load, Fig. 4, and therefore it would be expected that the fracture would originate at that notch and propagate towards the opposite one. It was found, however, that the specimens with the notch depth $a = 20$ mm did not fracture in this manner, but crushed immediately under the loading points. The specimens with notches deeper than 20 mm fractured between the notches and only these results will be discussed here.

The load–deflection graphs (not included in this report) showed a linear relationship up to the peak load at which the sudden failure occurred. The load–deflection curves were evaluated according to ASTM E 399-83 [27], where this type of failure is classed as "brittle" and the maximum load at failure, P_{max}, was used to calculate the fracture parameter K_I from Equation 2. Table IV gives a summary of the results and indicates that the value of fracture toughness for soil–cement based on the discussed geometry varied between 0.11 and 0.17 MN m$^{-3/2}$. George [28] carried out fracture tests on soil–cement using 76 mm × 76 mm × 286 mm notched beams in three-point bending and his values varied in the range 0.09–0.14 MN m$^{-3/2}$.

Considering that different geometries and loading arrangements were involved, the results were surprisingly close. This result is encouraging, but clearly more research on specimens of different sizes and under different loading conditions should be carried out before any value of the fracture parameter K_I for soil–cement can be used as a reliable design parameter.

The examination of fractured surfaces provided invaluable additional information about the fracture processes. The tensile fracture in cementitious materials is characterized by the development of the continuous crack pattern with the tip of the visible cracks which are often blunted by a zone of microcracks relative to the size of materials homogeneity. In the case of split-cube specimens the fracture surfaces examined after the failure could be described as "clean" and consisting of only one visible continuous crack with both halves fitting well together. Numerical analysis and the visual observation of fractured surfaces indicated that most likely the Mode I (tensile) failure was generated between two opposite notches.

3.2. Mode II testing and fracture parameters

There is much controversy surrounding Mode II (in-plane shear) failure mainly because there is only a limited amount of information available about this potentially dangerous mode. Generally, shear and punching shear failures are considered more critical and catastrophic than other types of failure because they occur suddenly without any visible warning signs. The understanding of a fracture process in a shear stress field and consequently the evaluation of related fracture parameters is still not fully understood and is widely debated.

Cube specimens, 100 mm × 100 mm, modified by four notches, were loaded as shown in Fig. 3, and punch-through mechanism was achieved by applying a uniform compression between the notches. The notch depth a varied between 30 and 45 mm in 5 mm increments and the notch spacing used in this investigation was $H = 30$, 40 and 50 mm. Twelve samples of each geometry were tested.

It was established that the specimens with $H = 30$ mm gave the most consistent results and only these will be discussed here. Fracture parameters were calculated using three different approaches. The fracture energy, G, approach requires the fracture energy to be calculated from the load–deflection records. The area under the load–displacement curve was measured and divided by the newly formed crack, i.e. $G = U/B(w - a)$, giving one fracture parameter. The stress intensity factor approach utilized Equation 3, which was determined from the numerical analysis. Because measurement of parameters K and G were made on each specimen, the applicability of linear elastic theory was tested by evaluating the stress intensity factor, K, from the relationship given in Equation 1, assuming plane strain conditions.

Fig. 8 indicates the variation of K_{II} values with a/w ratio obtained by different approaches, namely using Equations 1 and 3. As can be seen, the K_{II} values follow a very similar relationship with the variation between 0.31 and 0.45 MN m$^{-3/2}$. The reasonable agreement between K_{II} values obtained from these equations seems to support the assumption that non-linearity of soil–cement is not significant and that the LEFM approach may be applied in fracture studies

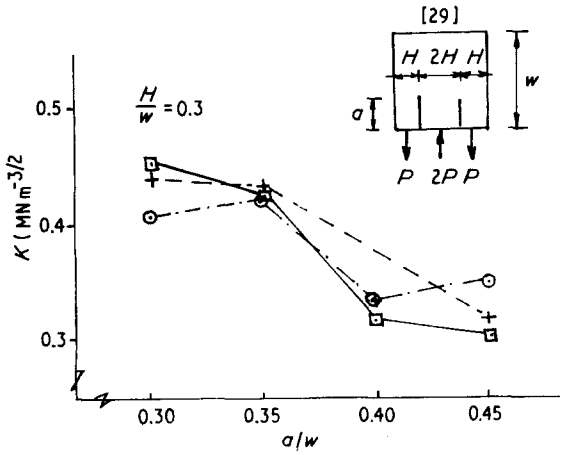

Figure 8 Comparison of fracture parameter K_{II} values determined by various methods. (+) Equation 1, (⊙) Equation 3, (⊡) Equation 4.

carried out on cube specimens discussed here.

The absence of any other work dealing with this mode of failure in soil–cement does not allow us a direct comparison of the independently obtained results. Chisholm and Jones [29] studied the Mode II failure mechanism on a specimen geometry shown in Fig. 8. They used a boundary collocation method in their analysis and the constitutive equation for the stress intensity factor was given as

$$K_{II} \cong \frac{Pw^{1/2}}{BH}\left(\frac{a}{w}\right)^{1/2} \quad (4)$$

This equation was used as an alternative method in assessing the order of magnitude of K_{II} values of soil–cement under the punch-through shear conditions. Fig. 8 also indicates the variation of these values with a/w ratio and it can be seen that the correlation of results is encouraging. Clearly more independent data and research, taking into account a possible size effect, are necessary before any conclusion regarding fracture parameters K_{II} in soil–cement can be drawn.

A visual inspection of the fractured surfaces indicated that very narrow crush zones consisting of fine microcracks developed between the top and bottom notches, following closely the directions of maximum shear stresses which were estimated by linear elastic stress analysis. The experiments also demonstrated that there were definite signs of abrasive action and that the parts of the specimen put together after the complete failure did not fit together. The mode of failure observed in these specimens was therefore assumed to be Mode II (in-plane shear). The comparison of the fracture response of split-cubes and punch-through shear specimens clearly indicated that two different types of failure were generated and that the corresponding fracture parameters were appreciably different in their magnitudes.

4. Conclusions

1. The sample preparation required closely controlled mixing, compacting and curing conditions in order to maintain a uniformity of soil–cement properties.

2. Two series of tests simulating Mode I and Mode II types of failure in soil–cement were discussed. The eccentrically loaded double-notched cubes were used in determining the fracture toughness parameter K_I in Mode I and it was found that this value was in the range 0.11–0.17 MN m$^{-3/2}$. The punch-through shear specimens were used in determining the fracture parameter K_{II} in Mode II, and this value was found to be between 0.31 and 0.45 MN m$^{-3/2}$.

3. It was observed that the fracture behaviour of soil–cement samples under tensile and concentrated shear loading were distinctly different and this was reflected by the values of the fracture parameters K_I and K_{II}. The stress intensity factor, K_{II}, was found to be about three times higher than K_I, a result contradicting assumptions that cementitious materials are generally weak in shear.

4. It was shown that the LEFM approach was applicable in this study, and both fracture parameters, K_{II} and G_{II}, could be used as a measure of the resistance of material to cracking. The consequence of this may be that the relationship $K^2 = GE/(1 - \nu^2)$ could be used as an alternative method in the determination of Young's modulus in soil–cement.

5. The sample geometry for both Mode I and Mode II fracture testing is simple and can be produced and tested in most materials laboratories. The insertion of notches must be carried out with a high degree of accuracy to ensure a uniformity of results.

6. It was demonstrated that the fracture mechanics approach can be an effective tool with which to study the cracking responses of soil–cement under different loading conditions. Clearly more research should be done to develop test procedures which would improve the understanding of fracture processes in this material and also to provide reliable fracture parameters that could be used in the design of this subbase material.

References

1. G. R. IRWIN, "Fracture mechanics" (Pergamon Press, 1960) pp. 557–92.
2. M. F. KAPLAN, *J. A.C.I.* **58** (1961) 591.
3. Z. BAZANT, *Mater. Construct.* **16**(93) (1983) 155.
4. P. F. WALSH, *Indian Concr. J.* **46** (1972) 469.
5. J. H. BROWN, *Mag. Concr. Res.* **24**(81) (1972) 185.
6. M. WECHARATANA and S. P. SHAH, *J. EMD ASCE* **109** (1983) 1231.
7. M. HILLERBORG, MODEER and P. E. PETERSON, *Cem. Concr. Res.* **6** (1976) 773.
8. Z. BAZANT and P. A. PHEIFFER, in "Proceedings of the 2nd Symposium on the Interaction of non-nuclear munitions with structures", Panama City Beach, Florida, April (Private Communication, 1985).
9. J. G. ROTS and RENE DE BORST, *J. Engng Mech.* **113** (1987) 1739.
10. Z. P. BAZANT and P. A. PHEIFFER, *Mater. Construct. (RILEM)* **19** (1986) 111.
11. A. R. INGRAFFEA and W. GERSTLE, "Application of Fracture Mechanics to Cementitious Composites" (Martinus Nijhoff, Dordrecht, 1985) pp. 247–85.
12. Y. S. JENG and S. P. SHAH, *J. Engng Mech. ASCE* **111** (1985) 1227.
13. K. VISALVANICH and A. E. NAAMAN, *J. EMD ASCE* **107** (EM6) (1981) 1155.
14. Z. P. BAZANT, *J. Engng Mech. ASCE* **110** (1984) 518.

15. Z. P. BAZANT and L. CEDOLIN, *J. Struct. Engng ASCE* **110** (1984) 1336.
16. Z. P. BAZANT and P. A. PHEIFFER, Center for Concrete and Geomaterials, Northwestern University, Evanston, Illinois, Report No. 86-8/428d (1986).
17. B. I. G. BARR and B. B. SABIR, *Mag. Concr. Res.* **37**(131) (1985) 88.
18. B. B. SABIR, PhD thesis, CNAA, London (1980).
19. J. DAVIES, T. G. MORGAN and C. W. YIM, *Int. J. Cem. Comp. Light. Concr.* **9**(1) (1987) 33.
20. J. DAVIES, *J. Mater. Sci. Lett.* **6** (1987) 879.
21. *Idem., Int. J. Cem. Comp. Light Concr.* **10** (1988) 3.
22. *Idem.*, "Fracture of Concrete and Rocks, Recent Developments" (Elsevier Applied Science, Cardiff, 1989) pp. 438–47.
23. *Idem.*, in "Proceedings of the 4th International Conference on Civil Engineering and Structural Engineering Computing", edited by B. H. V. Topping (Civil-Comp 89, London, 1989) pp. 351–60.
24. C. W. A. YIM, MPhil thesis, CNAA, London (1986).
25. BS1924: 1975, Methods of test for stabilised soils, Test 4 (British Standards Institution).
26. BS1881: Part 116 (British Standards Institution).
27. ASTM E 399-83, "Standard Test Method for Plane-Strain Fracture toughness" (American Society for Testing and Materials, Philadelphia, PA, 1984) pp. 519–54.
28. K. P. GEORGE, *Proc. ASCE J. Soil Mech. Founds.* **96** (1970) 991.
29. D. B. CHISHOLM and D. L. JONES, *Exp. Mech.* **17** (1977) 7.

Received 2 July
and accepted 1 November 1990